Fire Safety Journal 163 (2026) 104769

Contents lists available at ScienceDirect

Fire Safety Journal

journal homepage: www.elsevier.com/locate/firesaf

Influence of thermo-oxidative aging and thermal shock testing on the fire performance of high-Tg epoxy-based GFRP systems

Martin Demleitner [a], Quirin Niederauer [a], Bastian Treiber [a], Holger Ruckdäschel [a,b,*]

[a] Department of Polymer Engineering, University of Bayreuth, Universitätsstrasse 30, Bayreuth 95447, Germany
[b] Neue Materialien Bayreuth GmbH, Gottlieb-Keim-Straße 60, Bayreuth 95448 Germany

ARTICLE INFO

Keywords:
Fire behavior
Thermal shock
Thermo-oxidative aging
GFRP
Cone calorimetry

ABSTRACT

In fire-critical sectors like transportation and construction, flame-retardant composite systems must adhere to stringent safety standards. However, their long-term fire performance is often unexplored, as most studies assess fire behavior only in the as-received state, neglecting potential degradation due to environmental exposures. This study addresses this gap by examining the effects of thermo-oxidative aging and thermal shock testing on glass fiber reinforced composites, comparing both neat and flame-retardant modified version using aluminum diethyl phosphinate (AlPi). An initial assessment was carried out to identify the optimum concentration of AlPi and the impact of glass-fiber reinforcement on the fire behavior. Thermo-oxidative aging at 200 °C for 1000 h showed only slight effects. The maximum average rate of heat emission (MARHE) and effective heat of combustion (EHC) decreased, suggesting enhanced gas-phase flame inhibition and increased char stability. Visual inspections confirmed more stable char layers and reduced delamination in aged, flame-retardant composites. In contrast, thermal shock testing led to significant mechanical degradation, evidenced by up to a 30% reduction in interlaminar shear strength. This degradation is attributed to microcrack formation from internal stresses. Fire performance also deteriorated, with increases in MARHE and total smoke production (TSP) indicating more complete combustion.

1. Introduction

Various industries such as transportation, electronics, and construction demand materials that prevent or mitigate fire hazards and delay ignition. This is especially important for polymers, whose organic composition makes them mostly inherently flammable. Therefore, many polymers are modified with flame retardants to reduce flammability. These flame-retardant materials must meet various national and international fire safety standards, such as FAR25.853 for aircraft interior, EN45545-2 for railway applications, EN13501-1 for building materials and UL764A for electronics including the well-established UL94 test, before entering the market [1]. These standards focus on resistance to ignition, flame spread, heat emission and the release of toxic smoke.

However, fire behavior is typically tested only for virgin, unaged materials. As materials degrade over time due to environmental exposure, (e.g. temperature, UV radiation, humidity) their properties change. In many publications investigating various polymers (modified with flame-retardants), deterioration of the material is often only assessed in terms of thermo-mechanical and optical properties. Although the literature on the effects of different aging conditions on fire properties is limited, two reviews are focussing on this topic. Troitzsch elaborated in his recent review the impact of aging on the fire performance of polymers and coatings [2]. Furthermore, Vahabi et al. conducted a review with a particular focus on thermoplastic materials [3]. Under thermo-oxidative aging conditions, for long-fiber reinforced composite systems only thermoplastics based on polybutylene terephthalate (PBT) [4], polypropylene (PP) [5–8] or polyamide (PA6) [9,10] are mentioned. In these publications, regardless of the polymer, the Limiting oxygen index (LOI) increased due to aging. This was attributed to the carbonization of the thermoplastics and surface migration effects of the flame retardants, which contributed to the observed improvement in LOI. For heat release, the results vary significantly depending on the polymer and the flame retardant used. For long glass fiber-reinforced polypropylene with an intumescent flame retardant, the total heat release increased at 140 °C after 50 days of aging, from 103 to 127 MJ/m^2 [5]. In contrast, another study on long glass fiber-reinforced polypropylene reported a drastic decrease in total heat release under the same aging conditions, from 85.3 to 9.5 MJ/m^2 [7]. Unfortunately, no further explanation was given.

Thermoset resins, another class of polymers used in the aforementioned applications, have received less attention regarding the effect of

* Corresponding author at: Department of Polymer Engineering, University of Bayreuth, Universitätsstrasse 30, Bayreuth 95447, Germany.
E-mail address: ruckdaeschel@uni-bayreuth.de (H. Ruckdäschel).

https://doi.org/10.1016/j.firesaf.2026.104769
Received 16 October 2025; Received in revised form 23 February 2026; Accepted 23 March 2026
Available online 2 April 2026

aging on their fire performance. Their widespread adoption is driven by excellent specific mechanical properties, which make them well suited for lightweight transportation applications. In addition, they provide durability and corrosion resistance for construction purposes, as well as good thermal resistance, making them suitable for electronic housings and encapsulation. Phenolic resins are here an example which traditionally have been used due to their inherently good flame-retardant properties, which often require little to no additional flame retardants. However, several drawbacks such as relatively low mechanical performance, processing difficulties and health risks related to formaldehyde emissions, have raised concerns about phenolic resins. As a result, there is a growing trend towards using alternative systems, such as polyester or epoxy resins, that are modified with flame retardants.

The halogenated flame retardant 2,2',6,6'-Tetrabromo-4,4'-isopropylidenediphenol (TBBPA) has often been used in epoxy and polyester resins. TBBPA is one of the few halogenated flame retardants still on the market, as it is covalently built into the polymer network, which prevents migration and subsequent environmental contamination [11,12]. However, due to increasing restrictions and bans (e.g., REACH regulation, Stockholm convention) and growing environmental concerns, a shift towards alternative, halogen-free flame retardants is becoming increasingly evident. Prominent alternatives include organic flame retardants (phosphorus- or nitrogen-based) as well as inorganic options, such as aluminum hydroxide (ATH) or zinc-based compounds.

These flame retardants also demonstrate better thermo-oxidative stability compared to halogenated flame retardants, which tend to cause greater degradation of the resin matrix. However, for certain phosphorus- and nitrogen-based flame retardants, hydrolytic degradation can be more pronounced and should be taken into consideration [13,14].

In general, studies on the effects of aging on fire performance of thermoset resins remain limited. Most existing research has focused on thermoset-based fire-resistant coatings applied to steel substrates [15–18]. Jimenez et al. investigated an epoxy-based intumescent coating using a custom-built furnace test with a 35 kW burner [15]. The temperature rise during propane burner immersion on the back of the coated steel plate was measured. They compared the unaged resin with the aged resin (exposed to 80 °C and 70% relative humidity for 2 months), where no noticeable effect was observed between the samples.

To the best knowledge of the authors, the only study investigating the influence of thermo-oxidative aging on the fire resistance of thermoset composites via cone calorimetry was conducted by Sandinge et al. [19] They examined basalt fiber-reinforced phenolic resin systems, aging them at 90 °C for up to four weeks. Here, the peak heat release rate (PHRR) increased by 12%, total heat release (THR) increased by 44%, and total smoke production (TSP) increased by 34% while the time to ignition remained around 38 s, independent of aging. However, the details of the underlying mechanism remain unclear.

In addition to thermo-oxidative aging, rapid and extreme temperature fluctuations, also known as thermal shock, pose another significant challenge to composite materials. Typical areas where materials are exposed to thermal shock include, for example, aviation (engine components, brakes, and landing gear [20]), space (re-entry into the atmosphere [21]), and electronics (rapid power changes [22,23]). Thermo-shock induces high internal stresses at the fiber–matrix interface due to the mismatch in coefficients of thermal expansion (CTE) between the resin and the fibers, which can lead to microcracks and delamination [24–26]. The internal stress can be calculated by Eq. (1):

$$\sigma_m = \frac{E_m V_f E_f \left(\alpha_f - \alpha_m\right) \Delta T}{V_f E_f + V_m E_m} \tag{1}$$

where σ_m is the stress generated in the matrix, E_m and E_f are the moduli of matrix and fiber, α_m and α_f are the coefficients of thermal expansion for matrix and fiber, V_m and V_f are the specific volume content and ΔT is the temperature change [27,28]. Although there are various investigations on the influence of thermal shock on the mechanical properties of composites [29–31] no research addressing the influence on fire performance could be found.

Therefore, the aim of this study is to investigate the influence of thermo-oxidative aging and thermal shock on an epoxy-based glass-fiber-reinforced polymer (GFRP) composite system. Initially, the effects of the AlPi flame retardant and glass fiber reinforcement on fire performance were examined. Following aging at 200 °C for 1000 h and thermal shock testing over 100 cycles, the impact of composite degradation on mechanical properties and fire performance using cone calorimetry was evaluated.

2. Material & methods

The multifunctional semi-solid Novolac epoxy resin *Epiclon HP-7250* (DIC Corporation, Tokyo, Japan) with an epoxy equivalent weight (EEW) of 162 was used. Due to its high aromaticity and a functionality of ≥ 3.5, high glass transition temperatures up to 330 °C can be achieved. The resin has previously been investigated as a matrix material for composite components and extrusion-based additive manufacturing, particularly for high-temperature applications [32,33].

As curing agent, micronized 4,4-diaminodiphenyl sulfone (4,4-DDS) *Technicure K-10* provided by Acci Speciality Materials (Linden, NJ, USA) with a particle size of D_{50}=10 μm was used. The amine hydrogen equivalent weight (AHEW) of the curing agent is 62 resulting in an mixing ratio of 100:38.

As flame retardant, aluminum diethyl phosphinate AlPi distributed by Clariant AG (Muttenz, Switzerland) under the brand name *Exolit OP935* with a particle size of D_{50}=10 μm was used. Due to its high phosphorus content of 23 wt%, the flame retardant provides effective flame retardancy even at relatively low filler loadings. In combination with its fine particle size, the flame retardant is particularly suitable for composite applications and has also been utilized in the production of printed circuit board substrates [34,35]. Furthermore, phosphinate salts are not very susceptible to aging and hydrolysis, have a high temperature stability and maintain the fire performance even after prolonged water immersion [2]. In this study, concentration of AlPi was varied up to 20% by weight.

Fig. 1 shows the chemical structure of the used resin system and flame retardant.

Resin, curing agent, and, in the case of the modified system, flame retardant AlPi were homogenized at 120 °C for 20 min using a vacuum dissolver VMA Getzmann Dispermat (Reichshof, Germany). The resulting mixture was poured into preheated vertical molds at 120 °C, and the curing cycle was carried out in a convection oven *Memmert ULE 400*. It consisted of the following steps: 1 h at 120 °C, 3 h at 180 °C and an additional post-curing step for 2 h at 250 °C all with heating rates of 3 K/min. The cooling to room temperature took additional 8 h at a cooling rate of 1 K/min. The curing cycle was designed and monitored using differential scanning calorimetry (DSC) measurements of the cured samples. Since no residual enthalpy was detected up to 350 °C, the samples were considered fully cured.

For the composite specimen, prepregs were first manufactured. For this purpose, the resin was mixed with the curing agent and the additives, and then homogenized as previously described. With the prepreg impregnation unit *EHA Composite Machinery* the aero-grade fiberglass weave 8HS fabric *7781* (Porcher Industries Germany GmbH, Erbach, Germany) with an areal weight of 296 g/m^2 was impregnated. The calendar temperature was set to 80 °C aiming for a target prepreg areal weight of 440 g/m^2. The prepregs were subsequently cut, and eight plies were stacked in a [0/45/−45/90]s layup, resulting in a laminate thickness of 2 mm. Curing was performed under autoclave conditions at 6 bar, following the same curing cycle used for the neat resin samples. A fiber volume content of 50 vol.% was determined using density measurements (based on DIN EN ISO 1183) and thermogravimetric analysis (TGA), heating the samples in air up to 800 °C to fully pyrolyze the resin, leaving only the glass fibers.

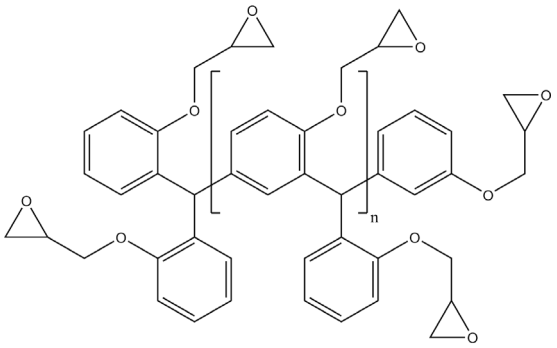

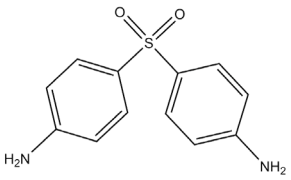

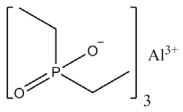

Fig. 1. Chemical structure of the components used in this study to formulate the resin systems.

Cone calorimetry

Fire behavior was evaluated using an iCone cone calorimeter (Fire Testing Technology Ltd., East Grinstead, UK). The tests were conducted in accordance with DIN ISO 5660. Sample size is 100 mm x 100 mm with a thickness of 3 mm for resin systems and thickness of 2 mm for composite systems. The samples were wrapped in an aluminum foil pocket and placed in a metal frame sample holder, which exposed 88.4 cm^2 of the sample surface. Insulation in the form of rock wool was placed beneath the specimen and additionally used to press the specimen against the upper part of the metal frame holder. The samples were irradiated at a distance of 25 mm with a heat flux of 35 kW/m^2. These parameters were chosen based on the conditions specified for testing interior aircraft materials to fulfill the requirements of the aviation standard FAR 25.853.

To ensure reproducible results, the end of the measurement was defined as the point at which the heat release rate stabilized, but not earlier than 60 s after flameout. Each resin and composite system was measured at least two times.

Mechanical testing

Apparent interlaminar shear strength of the GFRP was determined according to standard DIN EN 2377. The dimensions of the test specimens are 20 x 10 x 2 mm^3. The span was set for each specimen to be five times the specimens thickness.

The interlaminar shear strength is calculated by

$$\tau_{\mathrm{ILSS}} = 0.75 \cdot \frac{F_m}{B} \cdot d \tag{2}$$

where F_m is the maximum compressive force, B is the specimen width, and d is the specimen thickness. At least five specimen for each data set were tested.

Flexural properties were carried out in accordance with DIN ISO 14125 standard. The dimensions for the GFRP specimens were set at 60 × 15 ×2 mm^3 with a support span of 40 mm. Testing was conducted using a zwickiLine Z2.5 universal testing machine (ZwickRoell GmbH & Co. KG, Ulm, Germany).

Glass transition temperatures T_g of the resin and composite systems before and after thermo-oxidative aging and thermal shock tests were measured according to DIN EN ISO 6721-1. A rheometer RDA III (Rheometric Scientific) was used for the measurements with a heat ramp of 3 K/min, frequency of 1 Hz and strain of 0.1% and sample size of 50x10x2 mm^3. T_g was taken as the peak of the loss factor peak tan(δ).

Aging experiments

Thermo-oxidative aging was carried out in a standard convection oven (Memmert UF500) for 1000 h at 200 °C on composite systems and the weight loss recorded. The aging temperature was selected based on a previous study, in which 200 °C was determined as a temperature that balances significant thermo-oxidative aging effects without causing excessive deterioration of overall performance [36]. Furthermore, 150–180 °C, sometimes extended to 200 °C for advanced systems, is commonly considered the upper temperature limit for various epoxy resin systems [37,38].

In addition, thermal shock test were carried out. Thermal shock was selected as it is more severe than standard thermal cycling, resulting in increased stresses on the material. A two-chamber system was used, allowing the samples to be automatically transferred between the hot and cold zones. The Weiss ShockEvent T60/V2 from Weiss Technik GmbH (Reiskirchen, Germany) was utilized for this purpose. The hot chamber was set to 200 °C, and the cold chamber was set to −50 °C. The temperature range was selected based on assumed worst-case scenario for aviation parts, with outdoor temperatures of −50 °C at ground level or at high altitude rapidly rising to 200 °C, for example in components located close to the engine. Furthermore, the maximum temperature was selected based on literature values, where thermal shock testing is typically conducted at 60%–90% of the glass transition temperature [39,40]. The initial T_g of the resin system in this study is around 320 °C, therefore, 200 °C was selected in alignment with the temperature chosen for continuous thermo-oxidative aging. A total of 100 cycles were carried out. According to DIN EN 60068-2, 15 min are allotted for temperature equalization during chamber switching, with an additional 15 min to ensure the specimens reach the target temperature. This results in a total duration of 60 min per cycle, which is equivalent to 250 h in total.

Micro X-ray computed tomography (μ-CT)

Selected ILSS specimens were scanned via μ-CT to check the influence of thermal shock on microcrack and delamination formation. All scans were performed on the micro-CT system phoenix v|tome|x s 240/180 research edition from Baker Hughes Digital Solutions GmbH (software phoenix datos|x 2 acquisition 2.5.1). Scanning parameters were 50 kV voltage, 250 µA current, 1000 ms time, generating 1800 images with a voxel size 12.5 µm. The reconstructed volumes were processed using the manufacturer's software (phoenix datos|x 2 reconstruction v2.5.1). The threshold separating the material from the background was set to 0.12 ± 0.01 absorption coefficient. The 3D images were created were subsequently generated using Volume Graphics VGStudio Max, and volume-related parameters were extracted from these datasets.

Table 1
Characteristic parameters by cone calorimetry for neat and AlPi-modified resin systems.

System	TTI	PHHR	MARHE	EHC	TSP	Residual mass	FRI
	s	kW/m^2	kW/m^2	MJ/m^2	m^2	%	/
Neat resin	103 ± 1	857 ± 8	236 ± 5	19.3 ± 0.0	15.3 ± 0.3	34.7 ± 2.3	–
5% AlPi	98 ± 1	444 ± 1	136 ± 4	15.7 ± 0.6	17.2 ± 2	44.0 ± 2.8	2.6
10% AlPi	107 ± 4	392 ± 45	128 ± 5	15.6 ± 0.1	20.1 ± 1.9	46.0 ± 6.7	3.1
20% AlPi	105 ± 3	399 ± 25	132 ± 5	16.4 ± 0.3	18.0 ± 1.0	48.8 ± 1.9	3.0

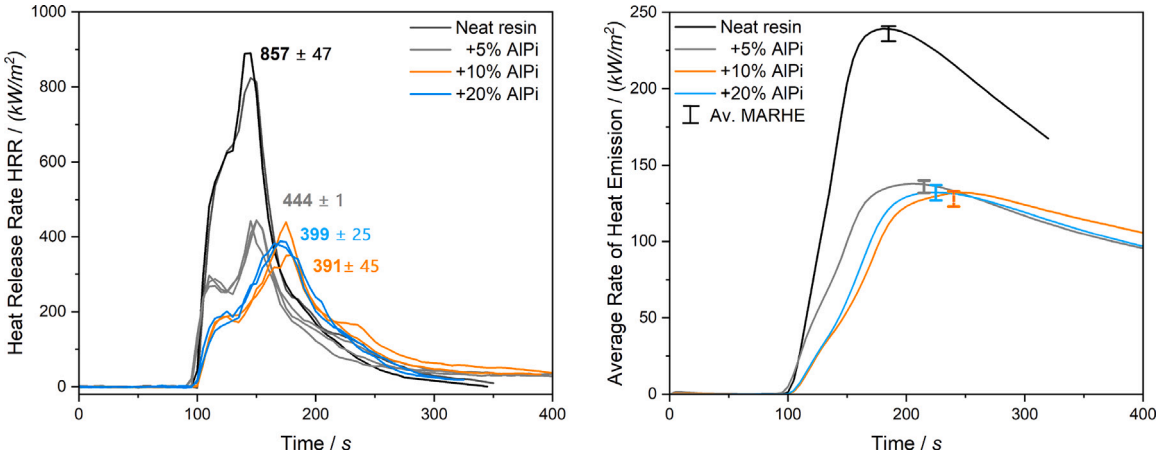

Fig. 2. Heat release rate HRR with PHRR(left) and average rate of heat emission with MARHE in dependence of AlPi content (right).

3. Results and discussion

Influence of flame retardant concentration

The AlPi content was systematically varied with selected concentrations of 5, 10 and 20% by weight and cone calorimetry measurements were carried out. The results of the most significant flame retardancy characteristic values, like time to ignition (TTI), peak heat release rate (PHHR), maximum average heat release rate (MARHE), effective heat of combustion (EHC), total smoke production (TSP), residual mass and flame retardancy index (FRI) are summarized in Table 1. The TTI stays rather constant around 100 s without significant impact of AlPi addition. This can be explained by the fact that the time to ignition primarily depends on the irradiated surface area relative to the overall volume, which is the same for all samples, as well as the thermal conductivity of the material. Both factors are considered not to be significantly influenced by the addition of AlPi.

Fig. 2 (left) shows the heat release over time. The peak heat release rate is significantly reduced by 48% with an addition of 5 wt% AlPi. Increasing the AlPi content from 5 wt% to 10 wt% yields only a marginal additional reduction of approximately 10% in PHHR.

The pHRR of the sample with 20 wt% AlPi falls within the error range of the results obtained with 10 wt% AlPi, indicating that the flame retardant's efficiency is limited and that increasing the loading to 20 wt% does not lead to further improvement. Similar limitations for AlPi in epoxy-based resin systems were reported recently [41]. All HRR curves of the AlPi-modified systems initially show a slight shoulder around 110 s before the fully developed fire occurs. Only a minor shoulder can be seen in the neat resin system, as the fire development is not inhibited. In addition, the time at which the pHRR is reached shifts to later points as the AlPi content increases, with 140 s for the neat resin, 150 s for 5 wt% AlPi, and a maximum of 175 s for 10 wt% AlPi content.

MARHE, depicted in Fig. 2, is a critical parameter that indicates how quickly and to what extent a material releases heat in the event of a fire. MARHE is influenced by TTI, PHRR, THR, and peak type and considers the average and cumulative effect of heat release in the combustion process therefore it reflects the general heat release performance. This means that not only the absolute HRR value plays an important role, but also the shape of the HRR curve. Fig. 2, right shows the ARHE curves and average MARHE values of the investigated resin systems. The later the PHRR occurs, the lower the ARHE [42]. The neat resin exhibits a MARHE of 236 kW/m^2 at an irradiance of 35 kW/m^2. This value is significantly lower than that of comparable resin systems. For example, a Novolac epoxy resin system (D.E.N. 438 with 4,4'-DDS) exhibited a MARHE of 326 kW/m^2, which is 38% higher [43]. This improved performance can be attributed to the high aromaticity of *Epiclon HP-7250*, which promotes increased char formation (residual mass under N_2 at 800 °C: 34.7% vs. 28% for D.E.N./4,4'-DDS). The resulting higher char yield acts as an effective thermal barrier, reducing further decomposition and heat release. Adding 10 wt% AlPi achieves the best MARHE value of 128 kW/m^2 after approximately 285 s. This corresponds to nearly a 50% reduction compared to the neat resin. The trend of the MARHE values corresponds to the time at which PHRR is reached. Similar to PHHR, a further addition of AlPi does not lead to improved MARHE.

The effective heat of combustion (EHC) is defined as the total heat evolved (THE) divided by the total mass loss (TML), representing the heat released per unit mass lost in the cone calorimeter. EHC is commonly used to evaluate the efficiency of a flame retardant, particularly in terms of flame inhibition and gas-phase activity. Thereby, a lower EHC indicates more effective gas-phase activity. EHC is drastically reduced by more than 20% by adding 5 wt% AlPi in comparison to neat resin. Further adding AlPi and hence increasing the phosphorus content leads to no improvement and with 20 wt% rather to a reverse effect of reduced efficiency as was shown by Rabe et al. [44] Here, the ability to release phosphorous radicals into gas-phase is restricted and cannot contribute to further gas-phase activity during burning due to charring effects that inhibit its action.

As anticipated, the incorporation of AlPi promotes flame inhibition, resulting in more incomplete combustion and consequently higher total smoke production (TSP). Total smoke production (TSP) reaching a maximum with of 20.1 m^2 with 10 wt% AlPi, an increase of 32% compared to the neat resin. This change from predominant gas-phase activity at 5 wt% to condensed-phase activity at 10 and 20 wt% can be seen in the surfaces of the cone specimen after testing, visible in Fig.

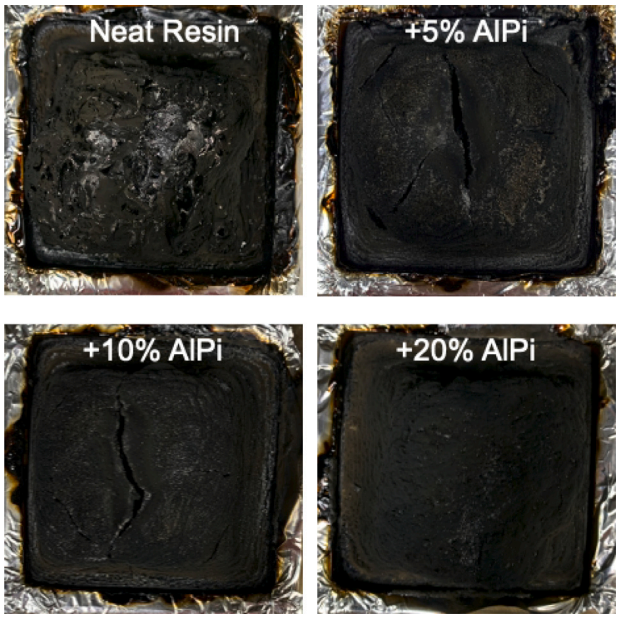

Fig. 3. Surface of resin system specimens with varying amounts of AlPi after cone calorimetry tests.

3. The neat resin shows a porous structure with bubbles and cracks indicating unstable char formation. With increasing AlPi content, a more stabilized char layer forms, shielding the epoxy resin from heat and preventing the outgassing of combustible gases. This leads to a delayed PHRR and an increased residual yield, from 34.7% for the neat resin to 48.8% for the system with 20 wt% AlPi. Compared to that, the system with 10 wt% AlPi exhibits the lowest EHC value and a high char yield, indicating a good balance between gas-phase and condensed-phase activity.

Besides MARHE, another parameter for rating the general effectiveness compared to the neat resin is the flame retardance index (FRI) [45, 46]. FRI is defined as the product of total heat release (THR) and pHRR, divided by TTI (Eq. (3)). According to Vahabi, an FRI below 1 indicates poor flame-retardant performance, between 1 and 10 indicates good performance, and above 10 indicates excellent performance [47].

$$\mathrm{FRI} = \frac{\left(\mathrm{THR} \cdot \frac{\mathrm{pHRR}}{\mathrm{TTI}}\right)_{\mathrm{ref}}}{\left(\mathrm{THR} \cdot \frac{\mathrm{pHRR}}{\mathrm{TTI}}\right)_{x}} \tag{3}$$

Adding 5% AlPi results in an FRI of 2.6, while increasing the loading to 10% improves the FRI to 3.1. However, adding 20% shows no further improvement, as already observed for MARHE and EHC.

The relative efficiencies of the amount of AlPi for PHRR, MARHE and TSP are summarized in Fig. 4. A clear reduction in relative efficiency is visible with increasing AlPi content. These results illustrate that, starting from 5 wt%, further addition of AlPi beyond 10 wt%, hardly improves the results. At 20 wt% AlPi, for each percent of AlPi a mere reduction of 2% of PHHR and MARHE is visible. Therefore, apart from processability issues from increased viscosity, further addition of the flame retardant offers no significant gain in flame-retardant efficiency. Hence, a loading of 10 wt% AlPi was selected for composite manufacturing as it provides an optimal balance between flame-retardant performance and processability on the neat resin level.

Influence of glass-fiber reinforcement

In Fig. 5 the influence of the glass fiber reinforcement on the heat release is compared to the neat resin systems. The neat GFRP system shows the typical HRR curve of a highly flammable material,

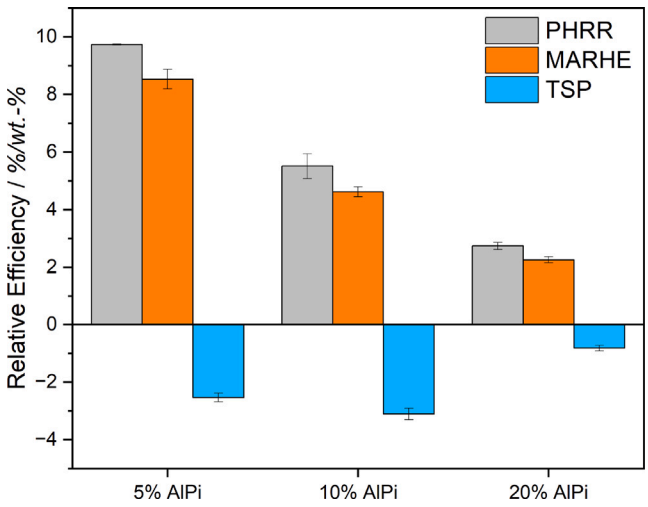

Fig. 4. Relative Efficiency of AlPi on PHRR, MARHE and TSP compared to the neat resin.

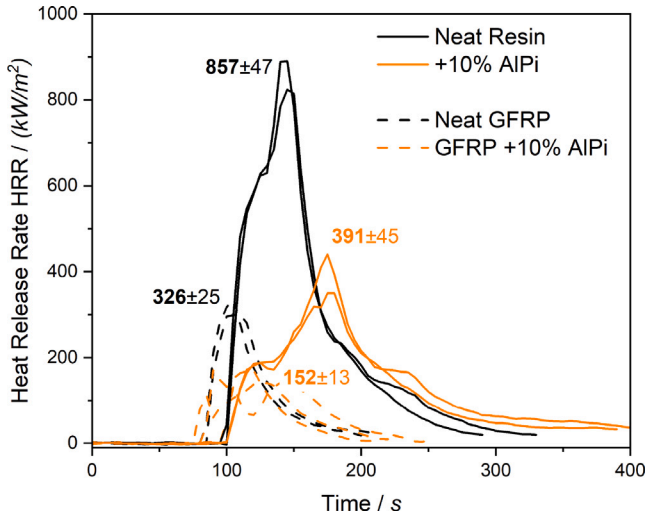

Fig. 5. Heat release rate over time for the investigated resin and composite systems.

with a sharp increase after ignition followed by a rapid decrease as the material is consumed. In contrast, the AlPi-additivated system is characterized by an initial rise in heat release rate, followed by a plateau. This behavior is attributed to the formation of a char layer, which protects the underlying material and prolongs heat release at significantly lower levels.

The fiber reinforcement leads to a reduction of approximately 62% in PHRR for both the neat and flame-retardant GFRP systems compared to the corresponding resin systems. However, considering that the fiber content is around 70 wt%, this reduction is primarily due to mass replacement with non-combustible glass fibers and actually indicates a deterioration in the fire behavior of the resin matrix itself. This phenomenon is well-known in the literature [48–50], as the fibers act as capillary pathways, known as the "wick effect", for flammable gases, leading to faster ignition. In the case of the GFRP systems, ignition occurred approximately 20 s earlier compared to the resin systems. Furthermore, since E-glass fibers have a higher thermal conductivity (~1.0–1.3 W/m K) [51] compared to the resin system (~0.2 W/m K) [52], they facilitate better heat transmission to the underlying material during cone calorimetry measurements. The fire properties measured via cone calorimetry of the GFRP systems are summarized in

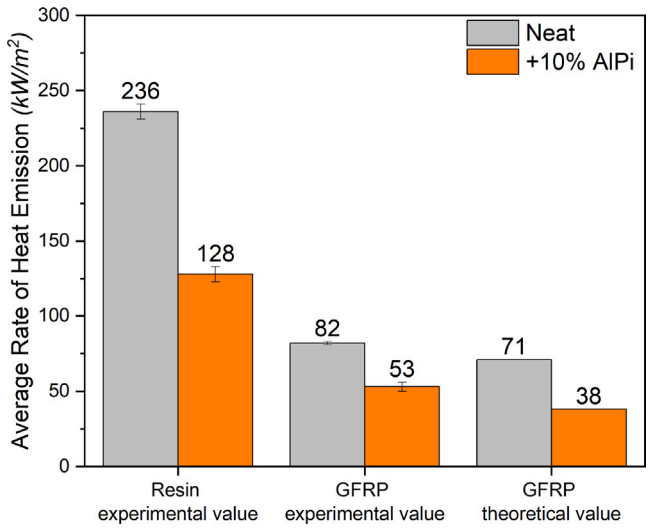

Fig. 6. Comparison of MARHE of neat resin and experimental and theoretical value based on glass fiber content.

Table 2. The heat release rates of the resin and GFRP systems, shown in Fig. 5 and normalized to the resin content, are presented in the Supporting Information (S4), highlighting the deteriorated behavior of the GFRP system. The corresponding absolute and normalized mass loss rates for both systems are also provided. For MARHE, a similar reduction of 65% is observed between the neat resin and neat GFRP. For the AlPi-modified resin, a decrease of 59% is observed introducing glass fiber reinforcement. The slightly lower reduction in the AlPi-modified systems can be attributed to the diminished efficiency of AlPi in the presence of glass fibers. Assuming a purely linear effect of the reinforcement at a weight content of 70%, a theoretical MARHE value can be calculated. The comparison between experimental and theoretical values is shown in Fig. 6. For the neat GFRP system, the measured value is 18% higher, and for the GFRP + 10% AlPi system, the measured value is 29% higher than the theoretical value. This shows the deteriorating effect of glass fiber reinforcement on MARHE of the neat resin and the flame retardant resin system. This can be linked to suppressed gas-phase activity and increased, but less efficient, condensed-phase activity of AlPi.

The EHC of the neat GFRP system (19.5 kJ/m^2) is very similar to the neat resin system with 19.3 kJ/ m^2 indicating that the glass fibers do not support gas phase activity by flame inhibition or fuel dilution in gas phase. For the AlPi-modified systems, the EHC increases again by introducing glass fibers from 15.6 kJ/m^2 to 18 kJ/m^2. This result proves again suppressed gas-phase activity of AlPi in the composite system.

Regarding total smoke production, a reduction of approximately 70% was observed, from 15.3 to 4.5 m^2, upon the introduction of fiber reinforcement into the neat system. This reduction corresponds directly to the fiber content by weight. Interestingly, in the system GFRP+10% AlPi, an even greater reduction of 78% was achieved. Starting from a higher value of 20.1 m^2, due to more incomplete combustion, the introduction of glass fibers reduced total smoke production to 4.3 m^2. This suggests that glass fibers together with AlPi can counteract the increased smoke production typically caused by incomplete combustion, acting as an efficient smoke suppressant. As described in the literature, the AlPi residue, namely $AlPO_4$, effectively binds the char and fibers together, promoting the formation of a shielding layer that blocks further burning and smoke production [53,54].

Lastly, glass-fiber reinforcement leads to an FRI of 11.9 compared to the neat resin. For the resin with 10% AlPi, glass-fiber reinforcement almost doubled the FRI from 3.1 to 6.0. Nevertheless, it again shows that the introduction of fiber reinforcement results in a relative deterioration of flame-retardant properties of the modified resin system.

Influence of thermo-oxidative aging on the GFRP system

After thermo-oxidative aging at 200 °C for 1000 h a weight loss of approximately 2% was observed for the GFRP systems. This is consistent with a previous aging study on the same systems, which focused on weight loss and lifetime predictions and reported weight losses of approximately 3% [36]. However, that study employed a higher surface-to-volume ratio (SVR) of 1.8, compared to the SVR of 1.04 for the cone specimens used here. With a higher SVR, more surface area is exposed to oxidation, generally leading to increased weight loss. Thermo-oxidative aging results in oxidation and subsequent embrittlement of the matrix, chain scission, and degradation of the crosslinked resin network [55]. After aging, oxidation effects at the surface were assessed using fluorescence microscopy (see Supporting Information S1). Here, the build-up of an oxidized layer of several hundred μm is visible.

Network degradation was furthermore evaluated by measuring the glass transition temperature (T_g) using Dynamic Mechanical Analysis (DMA) (see Supporting Information S2). For the GFRP systems studied here, a decrease in T_g from 317 °C to 292 °C (decrease of 8%) was observed. Furthermore, the effect of aging on the flexural properties was investigated and is shown in Fig. 7. Due to oxidation, the flexural moduli increased by 8% for both systems. The flexural strength decreased for the neat GFRP by about 8% and 23% for the AlPi-modified GFRP. Here, it seems that thermo-oxidative aging of the additivated system enhances stress concentration on the AlPi particles lowering further the flexural strength. The dominant failure mode was identified as tensile failure, characterized by pronounced cracks on the bottom surface. No change in the failure mechanism was observed due to thermo-oxidative aging compared to the unaged specimens. Elongation at break was reduced by around 12% for both systems due to oxidation based on reduced chain mobility and more brittle resin systems. In summary, influence of the thermo-oxidative aging on the thermo-mechanical properties is rather low with no drastic drop visible.

The results of the subsequent cone calorimetry tests are summarized and compared with the unaged specimens in Table 2. For the GFRP systems, it is noteworthy that TTI was not affected by aging in neither the neat nor the modified GFRP. Due to aging, network degradation normally leads to faster ignition because of earlier softening. However, the formation of an oxidized surface layer initially impedes heat transfer, delaying ignition. Since the influence of aging conditions on network degradation is considered rather low, evidenced by only a minor drop in T_g, and the oxidation layer might counterbalance these effects, the TTI remains constant. The minor reduction in total smoke production of the aged specimens can be attributed to weight loss and, consequently, a lower amount of burnable organic content.

For the neat GFRP system, a slight decrease of approximately 5% in the effective heat of combustion (EHC) is observed. With an increase in residual mass of around 2%, indicating more incomplete combustion, the reduction in EHC can be attributed to improved charring performance of the aged neat GFRP. This effect is likely due to oxidation of the composite and the formation of an oxidized surface layer, which helps stabilize the char. Notably, EHC decreases by 9% for aged AlPi-additivated system, which is nearly twice the reduction observed in the aged neat GFRP system. Since the residual yield increases by only 1.7%, similar to that of the neat GFRP, it appears that aging enhances both gas-phase flame inhibition and char formation.

PHRR remains unchanged for the neat GFRP system, whereas a 6% increase in PHRR is observed for the FR-modified GFRP. Despite this increase, the FR-modified system shows an 8% reduction in MARHE throughout flaming combustion. The changes due to thermo-oxidative aging on the heat release are shown in Fig. 8.

Consistent with the trends observed for the individual flame-retardant parameters, thermo-oxidative aging resulted in an FRI of 0.76 for the neat GFRP, reflecting a slight deterioration in flame-retardant performance relative to the unaged material. In contrast, the GFRP

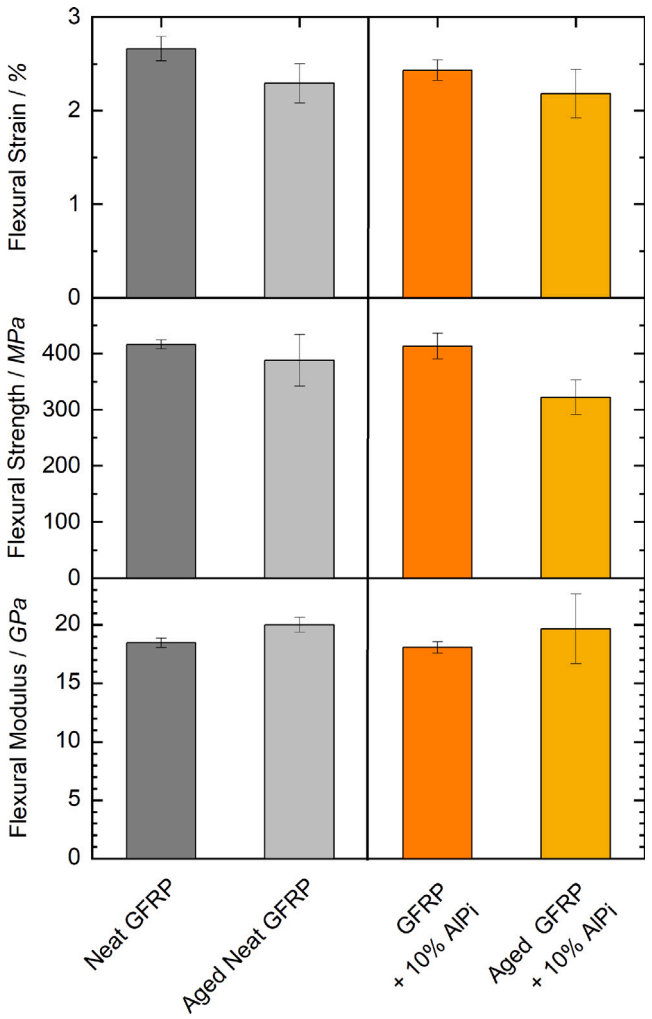

Fig. 7. Flexural Properties of the GFRP systems before and after 1000 h at 200 °C in air atmosphere.

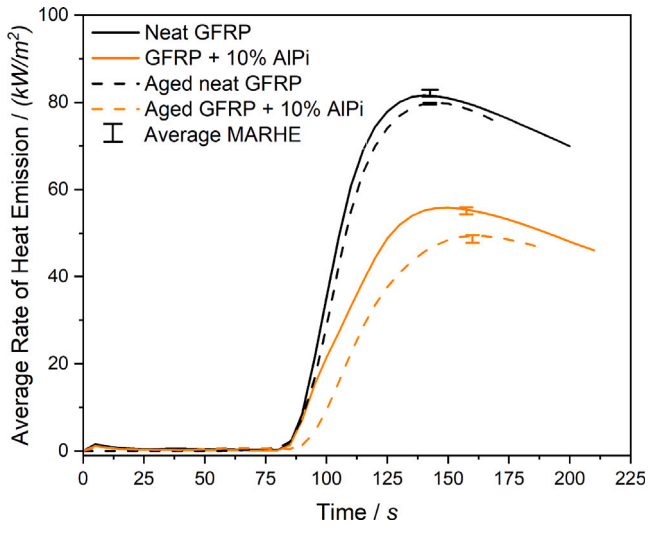

Fig. 8. Heat release rate over time for the GFRP systems before and after thermo-oxidative aging for 1000 h at 200 °C.

containing 10% AlPi exhibited a modest improvement, reaching an FRI of 1.6 following thermo-oxidative aging.

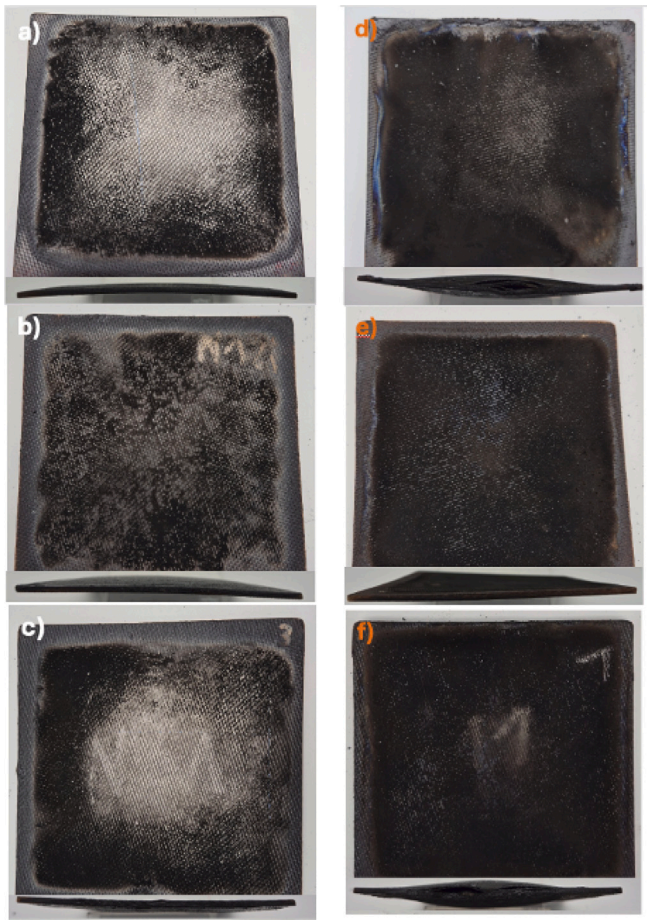

Fig. 9. Top and side view of neat GFRP (a–c) and GFRP+10% AlPi (d–f) of unaged (a, d) thermo-oxidative aged (b, e) and thermal shock-tested (c, f) cone calorimetry specimen after burning.

In Fig. 9, the front and side view of the unaged and aged specimen after cone testing are depicted. It can be observed that thermo-oxidative aging led to a more charred surface for both GFRP systems. This is especially evident when comparing the neat unaged GFRP system, where the remaining glass fibers are clearly visible, with the neat aged GFRP system, which shows more pronounced char residue.

Furthermore, in the FR GFRP system, the decomposition of AlPi in the gas phase during burning leads to higher swelling and delamination of the composites. This behavior is significantly reduced in the aged FR GFRP system, as oxidation appears to increase the delamination resistance between the plies.

Influence of thermal shock on the GFRP system

The influence of thermal shock testing on the flexural properties is presented in Supporting Information S3. The modulus increased only slightly, by 2% in the neat GFRP and 6% in the FR-modified GFRP system, while the flexural strength decreased by approximately 10% in both systems. The smaller increase in modulus after thermo-shock tests, compared to thermo-oxidative aging, can be attributed to the significantly shorter exposure time (50 h) at 200 °C. The impact of thermal shock, which appears to occur more on the macroscopic than on the molecular level, is further supported by the T_g measurements after thermal shock testing. Only a minor decrease in T_g was observed, from 317 °C to 310 °C in the FR GFRP and to 305 °C in the neat GFRP, indicating that the resin network remains largely unchanged.

Table 2
Characteristic flame retardancy values of the GFRP composite systems before and after thermo-oxidative aging and thermal shock testing.

System	TTI	PHHR	MARHE	EHC	TSP	Residual mass	FRI
	s	kW/m²	kW/m²	MJ/m²	m²	%	–
Neat GFRP	85 ± 2	326 ± 25	82 ± 1	19.5 ± 0.1	4.5 ± 0	81.0 ± 0.5	11.9[a]
Aged Neat GFRP	83 ± 2	330 ± 14	80 ± 0.1	18.8 ± 0.4	4.4 ± 0.4	83.1 ± 0.5	0.76
Thermal Shock Neat GFRP	87 ± 5	453 ± 37	104 ± 3.6	19.8 ± 0.1	6.6 ± 0.1	75.1 ± 0	0.38
GFRP + 10% AlPi	88 ± 8	152 ± 13	53 ± 3	18.0 ± 0.2	4.3 ± 0.5	84.9 ± 0.6	6.0[a]
Aged GFRP + 10% AlPi	90 ± 1	162 ± 4	49 ± 1	16.2 ± 0.5	4.0 ± 0	86.6 ± 0.1	1.6
Thermal Shock GFRP+ 10% AlPi	85 ± 1	240 ± 13	75.4 ± 1.2	16.8 ± 0.3	6.9 ± 0.1	79.6 ± 0	0.62

[a] Compared to neat resin and resin+10% AlPi.

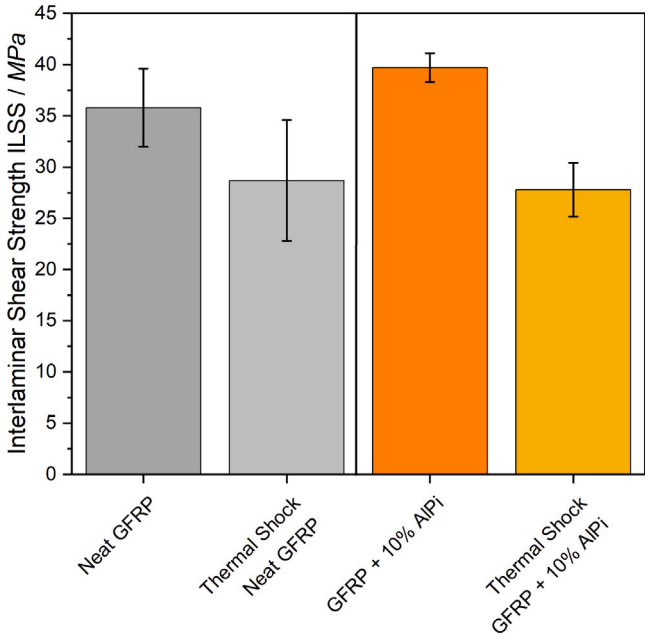

Fig. 10. Interlaminar shear strength of the GFRP systems before and after 100 cycles thermal shock testing.

Since flexural properties are in general strongly influenced by the surface condition of the specimen, oxidation has a greater impact on flexural performance compared to thermo-shock testing. However, thermal shock induces high internal stresses at the fiber–matrix interface leading to microcracks and delamination between plies. The effect of this internal stress during thermo-shock testing and stress relief via generating microcracks and delamination was measured via interlaminar shear testing (ILSS), a sensitive method for fiber–matrix bond quality and deterioration of interface properties [56–59]. Here, ILSS testing serves as an indirect method for microcrack formation as these are occurring on a μm length scale which is difficult to evaluate. The result can be seen in Fig. 10.

A drastic decrease in interlaminar shear strength is observed, with a 20% loss in the neat GFRP and a 30% loss in the GFRP with 10% AlPi after thermal shock testing. Using Eq. (1) and assuming a CTE of 5 μm/m K for the glass fiber and 50 μm/m K for the resin system, a temperature difference ΔT of 200 K and a modulus of ~ 72 GPa for E-glass fiber and 3.5 GPa for the epoxy resin, an internal stress of ~ 30 MPa in the resin matrix is generated. Although this is only a theoretical and highly localized internal stress, it highlights the stress induced by thermal shock in comparison with the measured shear strength. These drastic drops indicate severe formation of microcracks within the laminates due to thermal shock. In one of the few studies comparing thermal shock and thermo-oxidative aging of a carbon fiber-reinforced epoxy system under similar conditions for thermo-oxidative aging (150 °C for 600 h) and thermal shock testing (500 cycles between −50 °C and 180 °C), a significantly higher number of microcracks was observed in the thermally cycled specimen [60].

For deeper analysis on the influence of thermal shock on the GFRP system, μ-CT tomography measurements of the flame-retardant GFRP system before and after thermal shock were carried out. Side view of the specimen and the pore distribution is shown in Fig. 11. The unaged GFRP + 10% AlPi has an initial total porosity of 2.4% with pores in the range of 5–10 mm³. These pores can be linked to entrapped air during the manufacturing process of the GFRP composites. Considering the use of the highly viscous resin and woven fabric reinforcement, this porosity value reflects good processing conditions and is adequate for many applications, in which a maximum void content of 3% is commonly cited [61]. After thermal shock cycling, the total porosity increases almost by a factor of 4 to 9.3%. Here, it is visible that pore density as well as pore size increases with a typical pore size around 30–40 mm³. This increase is due to delamination tendencies connecting pores existing prior thermal shock and newly generated pores. Furthermore, as shown in Fig. 11 (middle), thermal shock led to a vast increase in small pores in the range below 0.1 mm³ and especially below 0.02 mm³. These pores likely originate from microcracks that develop along the matrix–fiber interface during thermal shock cycling.

The results of the fire performance of neat and FR GFRP systems after 100 cycles of thermal shock are summarized in Table 2. In contrast to thermo-oxidative aging, more pronounced deterioration of the flame-retardant properties is observed after thermal shock tests. The PHRR increased by 39% for the neat GFRP and by 58% for the AlPi-modified GFRP system. The MARHE increased similarly, by 27% for the neat GFRP, and 42% for the AlPi-modified GFRP system. The ARHE progression and the average MARHE of the thermal-shocked GFRP systems in comparison with the unaged GFRP systems are shown in Fig. 12. After thermal shock test aging, the overall indicator FRI shows a diminished flame retardancy performance, with a value of 0.38 for the neat GFRP and a slightly higher value of 0.62 for the GFRP containing 10%. Furthermore, a 6% reduction in residual mass coincides with smoke production increases of 46% in neat GFRP and 60% in the AlPi-modified GFRP.

The previously explained observations in the μ-CT measurements, ranging from microcrack formation to initial ply delamination can explain the overall deterioration in fire performance observed after thermal shock, in contrast to the comparatively minor impact on fire properties seen with thermo-oxidative aging. Cracks in the composite, especially on the interface, allow oxygen to penetrate more easily during combustion, resulting in a more sustained and accelerated burning process. Additionally, combustible gases can escape more readily through the damaged material, as the absence of a continuous oxidized surface layer no longer restricts their release. Thermal shock also reduces delamination resistance, making it easier for plies to separate during heat exposure. This, in turn, exposes underlying virgin material and increases the surface area exposed to fire, contributing to higher heat release. These effects, leading to more complete combustion, ultimately result in a lower residual yield after burning. Swelling and more advanced delamination are visible in the cone calorimetry specimen after thermal shock, as shown in Fig. 9.

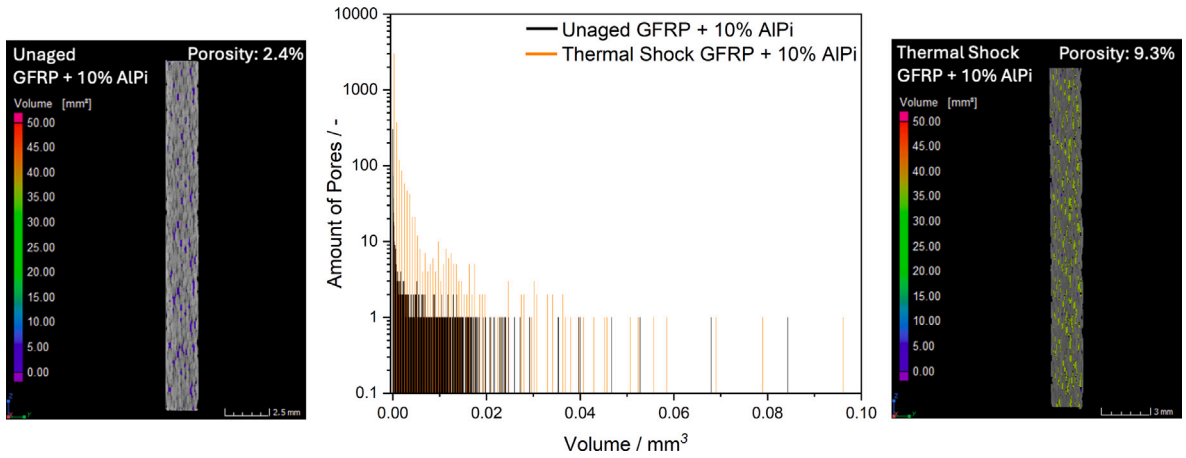

Fig. 11. Side view of μ-computed tomography images of unaged (left) and thermal shock (right) GFRP + 10% AlPi with pore distribution of small pores (middle).

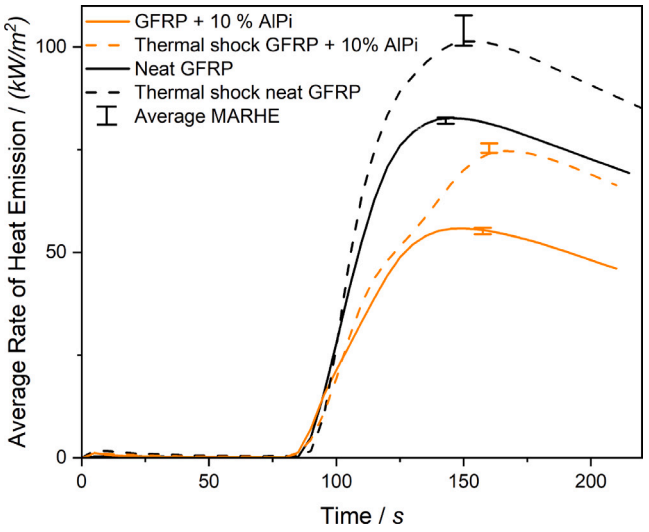

Fig. 12. Average rate of heat emission for the GFRP systems before and after 100 cycles of thermal shock.

4. Conclusion & outlook

In this work, the influence of environmental degradation, specifically elevated temperature of 200 °C and thermal shock tests, on the fire performance of a high-T_g epoxy-based GFRP system was investigated for the first time. To this end, the fire behavior of the samples was assessed using a cone calorimeter, both before and after thermo-oxidative aging and thermal shock testing respectively. Additionally, changes in mechanical properties, specifically flexural and interlaminar shear strength, were evaluated.

After 1000 h of thermo-oxidative aging at 200 °C, the flexural properties did not change significantly. A small increase in the modulus was observed due to oxidation and embrittlement, while flexural strength decreased by approximately 10%. The flame-retardant properties indicate that the fire performance of the samples can be well-preserved, or even enhanced, after thermo-oxidative aging. Specifically, both MARHE and EHC decreased, suggesting improved gas-phase flame inhibition and increased char stability. These findings were supported by enhanced charring and reduced delamination, particularly in the flame-retardant GFRP system.

Thermal shock tests (100 cycles between −50 °C and 200 °C) showed minor impact on the flexural properties but strong reduction of up to 30% in interlaminar shear strength. The degradation is attributed to microcrack formation caused by internal stresses resulting from differences in moduli and thermal expansion coefficients between the fiber and the matrix. μ-CT measurements of the GFRP + 10%AlPi system showed a drastic increase in total porosity both in small and medium sized pore range. Fire performance also deteriorated, with increased PHRR, MARHE, and smoke production by up to 60%, indicating more complete combustion, likely facilitated by the microstructural damage. This was further evidenced by a substantially lower residual yield after cone calorimetry.

The study demonstrated that aging has a clear impact on the long-term reaction-to-fire properties and should therefore be taken into account in every material development process. Based on these preliminary findings, further research is recommended to evaluate deeper the relationship between microcrack evolution and void content on the fire performance. In-situ coupling of cone calorimeter fire tests with GC–MS and FT-IR gas analysis can provide detailed insights into the impact of thermo-oxidative degradation on the composition of evolved gases and the chemical interactions occurring during combustion. Furthermore, different fiber lay-ups or other additives like toughenners or commonly used flame retardants for epoxy resins can be investigated, such as aluminum trihydrate (ATH) or 9,10-dihydro-9-oxa-10-phosphaphenanthrene-10-oxide (DOPO).

In summary, thermo-oxidative aging may enhance certain aspects of fire performance; however, thermal shock presents a more serious risk to the structural and fire safety of flame-retardant epoxy composites. These findings highlight the importance of considering both aging mechanisms in the design and evaluation of materials intended for fire-critical applications.

CRediT authorship contribution statement

Martin Demleitner: Writing – original draft, Validation, Investigation, Conceptualization. **Quirin Niederauer:** Writing – review & editing, Investigation, Formal analysis. **Bastian Treiber:** Writing – original draft, Validation, Investigation. **Holger Ruckdäschel:** Writing – review & editing, Supervision, Project administration, Funding acquisition, Conceptualization.

Declaration of competing interest

The authors declare that they have no known competing financial interests or personal relationships that could have appeared to influence the work reported in this paper.

Acknowledgments

The authors are grateful towards Florian Puchtler of the Chair of Inorganic Chemistry I at the University of Bayreuth for the introduction and support in the Cone calorimeter measurements.

We thank gratefully RCBE (Regensburg Center of Biomedical Engineering) for the support by μ-CT facility, and we acknowledge the support from the Deutsche Forschungsgemeinschaft (DFG) in frame of the program "Forschungsgeräte" (INST 102/11 – 1 FUGG).

Appendix A. Supplementary data

Supplementary material related to this article can be found online at https://doi.org/10.1016/j.firesaf.2026.104769.

Data availability

Data will be made available on request.

References

[1] M. Häublein, M. Demleitner, V. Altstädt, Fire behavior and flame-retardant properties of application-oriented fiber-reinforced polymers, Compos. Mater.: Manuf. Prop. Appl. (2021) 383–417, http://dx.doi.org/10.1016/B978-0-12-820512-9.00008-3,

[2] J.H. Troitzsch, Fire performance durability of flame retardants in polymers and coatings, Adv. Ind. Eng. Polym. Res. 7 (3) (2024) 263–272, http://dx.doi.org/10.1016/j.aiepr.2023.05.002.

[3] H. Vahabi, R. Sonnier, L. Ferry, Effects of ageing on the fire behavior of flame retarded polymers: A review, Polym. Int. 64 (2014) http://dx.doi.org/10.1002/pi.4841.

[4] H. Ye, J. Chen, C. Zhang, Z. Guan, Effect of thermoplastic toughening agent on phase separation and physicochemical properties of bismaleimide resin, in: 2017 8th International Conference on Mechanical and Aerospace Engineering, ICMAE 2017, ISBN: 9781538633052, 2017, pp. 79–84, http://dx.doi.org/10.1109/ICMAE.2017.8038621.

[5] N. Wang, X. Chen, K. Zhang, W. He, F. Qi, J. Guo, The influence of thermal oxidative ageing on flame retardancy, thermal and mechanical properties of LGFPP/IFR composites, J. Therm. Anal. Calorim. 131 (2) (2018) 1017–1024, http://dx.doi.org/10.1007/s10973-017-6679-4.

[6] Y. Wu, D. Xu, X. Chen, M.H. Min, Y. Zhou, W. He, J. Guo, Influence of thermo-oxidative aging on flame retardancy, thermal stability, and mechanical properties of long glass fiber–reinforced polypropylene composites filled with organic montmorillonite and intumescent flame retardant, J. Fire Sci. 37 (2) (2019) 176–189, http://dx.doi.org/10.1177/0734904119833014.

[7] N. Wang, X. Chen, J. Guo, D. Zhou, W. He, S. Ci, Effect of thermo-oxidative aging on the mechanical and flame retardant properties of long glass fiber-reinforced polypropylene composites filled with red phosphorus, Polym. Compos. 39 (8) (2018) 2634–2642, http://dx.doi.org/10.1002/pc.24253.

[8] J. Guo, M. Wang, L. Li, J. Wang, W. He, X. Chen, Effects of thermal-oxidative aging on the flammability, thermal degradation kinetics and mechanical properties of DBDPE flame retardant long glass fiber reinforced polypropylene composites, Polym. Compos. 39 (S3) (2018) E1733–E1741, http://dx.doi.org/10.1002/pc.24720.

[9] X. Zuo, H. Shao, D. Zhang, Z. Hao, J. Guo, Effects of thermal-oxidative aging on the flammability and thermal-oxidative degradation kinetics of tris(tribromophenyl) cyanurate flame retardant PA6/LGF composites, Polym. Degrad. Stab. 98 (12) (2013) 2774–2783, http://dx.doi.org/10.1016/j.polymdegradstab.2013.10.014.

[10] X. Zuo, H. Song, H. Shao, T. Wei, J. Guo, Aging of OMMT/halogen-antimony-filled LGFPA6 composite: Effect on static and dynamic mechanical properties and fire behaviors, Polym. Compos. 40 (6) (2019) 2208–2218, http://dx.doi.org/10.1002/pc.25026.

[11] B.K. Kandola, F. Magnoni, J.R. Ebdon, Flame retardants for epoxy resins: Application-related challenges and solutions, J. Vinyl Addit. Technol. 28 (1) (2022) 17–49, http://dx.doi.org/10.1002/vnl.21890.

[12] Y. Chen, J. Li, L. Chen, S. Chen, W. Diao, Brominated flame retardants (BFRs) in waste electrical and electronic equipment (WEEE) plastics and printed circuit boards (PCBs), Procedia Environ. Sci. 16 (2012) 552–559, http://dx.doi.org/10.1016/j.proenv.2012.10.076.

[13] C.-E. Wilén, R. Pfaendner, Improving weathering resistance of flame-retarded polymers, J. Appl. Polym. Sci. 129 (3) (2013) 925–944, http://dx.doi.org/10.1002/app.38979.

[14] R. Pfaendner, (Photo)oxidative degradation and stabilization of flame retarded polymers, Polym. Degrad. Stab. 98 (12) (2013) 2430–2435, http://dx.doi.org/10.1016/j.polymdegradstab.2013.07.005.

[15] M. Jimenez, S. Bellayer, B. Revel, S. Duquesne, S. Bourbigot, Comprehensive study of the influence of different aging scenarios on the fire protective behavior of an epoxy based intumescent coating, Ind. Eng. Chem. Res. (ISSN: 08885885) 52 (2013) 729–743, http://dx.doi.org/10.1021/IE302137G.

[16] Y. Dong, G. Wang, Q. Su, Influence of nano-boron nitride on anti-aging property of waterborne fire-resistive coatings, J. Coatings Technol. Res. (ISSN: 1935-3804) 11 (5) (2014) 805–815, http://dx.doi.org/10.1007/s11998-013-9538-7.

[17] L.L. Wang, Y.C. Wang, G.Q. Li, Q.Q. Zhang, An experimental study of the effects of topcoat on aging and fire protection properties of intumescent coatings for steel elements, Fire Saf. J. (ISSN: 0379-7112) 111 (2020) 102931, http://dx.doi.org/10.1016/j.firesaf.2019.102931.

[18] T.A. Roberts, L.C. Shirvill, K. Waterton, I. Buckland, Fire resistance of passive fire protection coatings after long-term weathering, Process. Saf. Environ. Prot. (ISSN: 0957-5820) 88 (1) (2010) 1–19, http://dx.doi.org/10.1016/j.psep.2009.09.003.

[19] A. Sandinge, P. Blomqvist, L. Schiøtt Sørensen, A. Dederichs, The effect of accelerated ageing on reaction-to-fire properties–composite materials, Fire Technol. 58 (2022) 1305–1332, http://dx.doi.org/10.1007/s10694-021-01197-9.

[20] A. Kubit, T. Trzepiecinski, M. Kłonica, M. Hebda, M. Pytel, The influence of temperature gradient thermal shock cycles on the interlaminar shear strength of fibre metal laminate composite determined by the short beam test, Compos. Part B: Eng. 176 (2019) 107217, http://dx.doi.org/10.1016/J.COMPOSITESB.2019.107217.

[21] K.I. Triantou, K. Mergia, B. Perez, S. Florez, A. Stefan, C. Ban, G. Pelin, G. Ionescu, C. Zuber, W.P.P. Fischer, J. Barcena, Thermal shock performance of carbon-bonded carbon fiber composite and ceramic matrix composite joints for thermal protection re-entry applications, Compos. Part B: Eng. (ISSN: 1359-8368) 111 (2017) 270–278, http://dx.doi.org/10.1016/J.COMPOSITESB.2016.12.020.

[22] X. Zhang, M. Wang, X. Li, Z. Ding, C. Ma, G. Lu, Y. Mei, A method for improving the thermal shock fatigue failure resistance of IGBT modules, IEEE Trans. Power Electron. (ISSN: 19410107) 35 (2020) 8532–8539, http://dx.doi.org/10.1109/TPEL.2019.2963236.

[23] Y. Kojima, T. Ohta, M. Matsushita, M. Takahara, T. Kurauchi, Thermal shock resistance of plastic IC package, J. Appl. Polym. Sci. 41 (1990) 2199–2206, http://dx.doi.org/10.1002/APP.1990.070410924.

[24] E.S. Folias, M. Hohn, Predicting crack initiation in composite material systems due to a thermal expansion mismatch, Int. J. Fract. (ISSN: 15732673) 93 (1998) 335–349, http://dx.doi.org/10.1023/A:1017160807854.

[25] F. Azimpour-Shishevan, H. Akbulut, M.A. Mohtadi-Bonab, Thermal shock behavior of twill woven carbon fiber reinforced polymer composites, J. Compos. Sci. 2021, Vol. 5, Page 33 5 (2021) 33, http://dx.doi.org/10.3390/JCS5010033.

[26] B.C. Ray, Thermal shock and thermal fatigue on delamination of glass-fiber-reinforced polymeric composites, J. Reinf. Plast. Compos. 24 (2005) 111–116, http://dx.doi.org/10.1177/0731684405042953.

[27] N.L. Hancox, Thermal effects on polymer matrix composites: Part 1. Thermal cycling, Mater. Des. 19 (3) (1998) 85–91, http://dx.doi.org/10.1016/S0261-3069(98)00018-1.

[28] S. Wang, Q. Li, W. Zhang, H. Zhou, Crack resistance test of epoxy resins under thermal shock, Polym. Test. (ISSN: 01429418) 21 (2002) 195–199, http://dx.doi.org/10.1016/S0142-9418(01)00069-1.

[29] S.J. Lu, T. Yang, X. Xiao, X.Y. Zhu, J. Wang, P.Y. Zang, J.A. Liu, Mechanical properties of the epoxy resin composites modified by nanofiller under different aging conditions, J. Nanomater. (ISSN: 16874129) 2022 (2022) http://dx.doi.org/10.1155/2022/6358713.

[30] S. Manjunath, K. U. Achutha, H. Sathyashankara, M.C. Gowrishankar, Investigation and optimization of thermal shock effects on the properties and microstructure of nanoclay-glass fiber reinforced epoxy composites, Mater. Res. Express (ISSN: 2053-1591) 6 (2019) 105360, http://dx.doi.org/10.1088/2053-1591/AB3F67.

[31] Z. Jamshidi, S.M. Hejazi, M. Sheikhzadeh, A. Alirezazadeh, Analysis of impacts of thermal shocks on mechanical properties of E-glass fiber reinforced polyester composites, J. Compos. Mater. 55 (2021) 3687–3698, http://dx.doi.org/10.1177/00219983211017648.

[32] M. Wimmer, B.G. Compton, Semi-solid epoxy feedstocks with high glass transition temperature for material extrusion additive manufacturing, Addit. Manuf. (ISSN: 22148604) 54 (March) (2022) 102725, http://dx.doi.org/10.1016/j.addma.2022.102725.

[33] C. Meier, P. Parlevliet, M. Döring, High temperature epoxy resins : Latent curing with various imidazoles and further enhancement of the mechanical and flame retardant properties, Thermosets 2015 (September 2015) (2016).

[34] J.D. Boysère, A. Beard, Halogen-free laminates: Worldwide trends, driving forces and current status, Circuit World (ISSN: 03056120) 32 (2006) 8–11, http://dx.doi.org/10.1108/03056120610642842.

[35] D. Goedderz, E. Chalwatzis, F. Schönberger, M. Döring, Flame retardant epoxy thermosets for electrical and electronic applications, Non-Halogenated Flame-Retardant Technol. Epoxy Thermosets Compos. (2024) 375–400, http://dx.doi.org/10.1016/B978-0-443-16046-2.00015-8,

[36] M. Demleitner, L. Endner, H. Ruckdäschel, Lifetime prediction of thermo-oxidative degradation of a modified epoxy resin and its glass fiber composite in air atmosphere and correlation with long-term aging behavior, Polym. Degrad. Stab. (ISSN: 0141-3910) 242 (2025) 111686, http://dx.doi.org/10.1016/J.POLYMDEGRADSTAB.2025.111686.

[37] P. Ren, L. Guozheng, Z. Zhang, Epoxy-modified cyanate ester resin and its high-modulus carbon-fiber composites, Polym. Compos. 27 (2006) 402–409, http://dx.doi.org/10.1002/PC.20207.

[38] C.P. Reghunadhan Nair, D. Mathew, K.N. Ninan, Cyanate ester resins, recent developments, Adv. Polym. Sci. (ISSN: 00653195) 155 (2001) 1–99, http://dx.doi.org/10.1007/3-540-44473-4_1,

[39] N. Zavatta, F. Rondina, M. Falaschetti, L. Donati, Effect of thermal ageing on the mechanical strength of carbon fibre reinforced epoxy composites, Polymers 13 (2021) http://dx.doi.org/10.3390/POLYM13122006.

[40] M.C. Lafarie-Frenot, S. Rouquie, Influence of oxidative environments on damage in c/epoxy laminates subjected to thermal cycling, Compos. Sci. Technol. 64 (2004) 1725–1735, http://dx.doi.org/10.1016/J.COMPSCITECH.2004.01.005.

[41] M. Friedel, J.V. Boehm, H. Ruckdaeschel, Impact of aluminum diethyl phosphinate (DEPAL) flame retardant on the thermal, mechanical, and fire-resistance properties of an amine-cured epoxy resin, J. Appl. Polym. Sci. 142 (21) (2025) e56923, http://dx.doi.org/10.1002/app.56923.

[42] A. Witkowski, A. Stec, T.R. Hull, Thermal decomposition of polymeric materials, in: M.J. Hurley, D. Gottuk, J.R. Hall, K. Harada, E. Kuligowski, M. Puchovsky, J. Torero, J.M. Watts, C. Wieczorek (Eds.), SFPE Handbook of Fire Protection Engineering, Springer New York, New York, NY, ISBN: 978-1-4939-2565-0, 2016, pp. 167–254, http://dx.doi.org/10.1007/978-1-4939-2565-0_7.

[43] M. Silveira, V.F. Moritz, C.A. Ferreira, L. Ferry, J. Lopez-Cuesta, Flammability of novolac epoxy cured with aromatic diamines, Thermochim. Acta 741 (2024) 179870, http://dx.doi.org/10.1016/j.tca.2024.179870.

[44] S. Rabe, Y. Chuenban, B. Schartel, Exploring the modes of action of phosphorus-based flame retardants in polymeric systems, Materials 10 (5) (2017) http://dx.doi.org/10.3390/ma10050455.

[45] M. Jauregui Rozo, S. Sunder, H. Ruckdäschel, B. Schartel, Char, gas, and action: Transfer of the flame-retardant modes of action in epoxy resins and their fiber-reinforced composites, Polym. Test. (ISSN: 0142-9418) 140 (2024) 108610, http://dx.doi.org/10.1016/J.POLYMERTESTING.2024.108610.

[46] F. Rothenhäusler, F. Ludik, L. Geiling, H. Ruckdaeschel, Flame retardant performance of phosphatized starch in epoxy resins: A sustainable approach to enhancing fire safety, J. Appl. Polym. Sci. 142 (2025) e57273, http://dx.doi.org/10.1002/APP.57273.

[47] H. Vahabi, E. Movahedifar, B.K. Kandola, M.R. Saeb, Flame retardancy index (FRI) for polymer materials ranking, Polym. (ISSN: 2073-4360) 15 (2023) 2422, http://dx.doi.org/10.3390/POLYM15112422.

[48] A.R. Horrocks, G. Smart, B. Kandola, D. Price, Zinc stannate interactions with flame retardants in polyamides; part 2: Potential synergies with non-halogen-containing flame retardants in polyamide 6 (PA6), Polym. Degrad. Stab. 97 (4) (2012) 645–652, http://dx.doi.org/10.1016/j.polymdegradstab.2012.01.004.

[49] T. Köppl, S. Brehme, F. Wolff-Fabris, V. Altstädt, B. Schartel, M. Döring, Structure-property relationships of halogen-free flame-retarded poly(butylene terephthalate) and glass fiber reinforced PBT, J. Appl. Polym. Sci. 124 (1) (2012) 9–18, http://dx.doi.org/10.1002/app.34910.

[50] B. Zhao, Z. Hu, L. Chen, Y. Liu, Y. Liu, Y. Wang, A phosphorus-containing inorganic compound as an effective flame retardant for glass-fiber-reinforced polyamide 6, J. Appl. Polym. Sci. 119 (4) (2011) 2379–2385, http://dx.doi.org/10.1002/app.32860.

[51] A. Goel, K.K. Chawla, U.K. Vaidya, N. Chawla, M. Koopman, Characterization of fatigue behavior of long fiber reinforced thermoplastic (LFT) composites, Mater. Charact. (ISSN: 1044-5803) 60 (2009) 537–544, http://dx.doi.org/10.1016/J.MATCHAR.2008.12.020.

[52] S. Bard, M. Demleitner, M. Radtke, V. Altstädt, Transverse thermal conductivity of epoxy carbon fiber prepreg laminates with a graphite filled matrix, J. Compos. Sci. (ISSN: 2504-477X) 3 (2019) 44, http://dx.doi.org/10.3390/JCS3020044.

[53] H. Seefeldt, E. Duemichen, U. Braun, Flame retardancy of glass fiber reinforced high temperature polyamide by use of aluminum diethylphosphinate: thermal and thermo-oxidative effects, Polym. Int. 62 (11) (2013) 1608–1616, http://dx.doi.org/10.1002/pi.4497.

[54] S. Brehme, T. Köppl, B. Schartel, V. Altstädt, Competition in aluminium phosphinate-based halogen-free flame retardancy of poly(butylene terephthalate) and its glass-fibre composites, E-Polymers 14 (3) (2014) 193–208, http://dx.doi.org/10.1515/epoly-2014-0029.

[55] J. Hübsch, M. Demleitner, S. S. Bard, P. Berendes, V. Altstädt, C. Mittelstedt, Influence of skydrol immersion at elevated temperatures on the thermo-mechanical properties of a high-t anhydride epoxy resin toughened with a hydroxy-terminated polyester, J. Appl. Polym. Sci. 140 (1) (2023) e53263, http://dx.doi.org/10.1002/app.53263.

[56] M. Sheikhzadeh, A. Alirezazadeh, Z. Jamshidi, S. Hejazi, A review on critical aspects of thermal shocks and thermal cycles in fiber reinforced polymer composites, J. Reinf. Plast. Compos. 42 (13–14) (2023) 656–672, http://dx.doi.org/10.1177/07316844221136569.

[57] A.P. Chakraverty, U.K. Mohanty, S.C. Mishra, B.B. Biswal, Effect of post-thermal shock on prolonged sea water aged GFRP composite, IOP Conf. Ser.: Mater. Sci. Eng. 115 (1) (2016) 12004, http://dx.doi.org/10.1088/1757-899X/115/1/012004.

[58] S. Sethi, B.C. Ray, Environmental effects on fibre reinforced polymeric composites: Evolving reasons and remarks on interfacial strength and stability, Adv. Colloid Interface Sci. 217 (2015) 43–67, http://dx.doi.org/10.1016/j.cis.2014.12.005.

[59] J. Ajaja, F. Barthelat, Damage accumulation in a carbon fiber fabric reinforced cyanate ester composite subjected to mechanical loading and thermal cycling, Compos. Part B: Eng. 90 (2016) 523–529, http://dx.doi.org/10.1016/j.compositesb.2015.09.054.

[60] M.C. Lafarie-Frenot, S. Rouquié, N.Q. Ho, V. Bellenger, Comparison of damage development in C/Epoxy laminates during isothermal ageing or thermal cycling, Compos. Part A: Appl. Sci. Manuf. 37 (4) (2006) 662–671, http://dx.doi.org/10.1016/j.compositesa.2005.05.002.

[61] F.Y.C. Boey, S.W. Lye, Void reduction in autoclave processing of thermoset composites: Part 1: High pressure effects on void reduction, Composites 23 (1992) 261–265, http://dx.doi.org/10.1016/0010-4361(92)90186-X.